Construction Approach of Deep Mountainous Tunnel Shaft having Interlacing Surrounding Rock Grades

Emmanuel Rukundo, Shen Yusheng, Zhou Pengfa, Zhu Shuangyan.

Abstract—Interlacing surrounding rock grades in a tunnel shaft poses challenges during construction; the study aims to determine the appropriate construction mechanics, secondary lining thickness and the safety factor. Based on Huayingshan mountainous tunnel shaft engineering for Nanchong- Dazhu-Liangping expressway in Southwest China. The circular shaft tunnel's internal force analytic solution was derived out. Meanwhile, using numerical methods, theoretical solutions are compared with numerical results. The safety factors were far higher than the specified safety factors, and slight bond strength between concrete and rock is sufficient to support the lining weight, making the underpinning construction technique more suitable. Therefore a combination of empirical calculations and numerical simulations proved helpful since the numerical analysis method can consider the coupling effects of some factors, such as varying rock properties and different excavation approaches.

Index Terms—Construction approach, Interlacing surrounding rock grades, Construction mechanics, Shaft engineering

1. INTRODUCTION

Geotechnical engineers have traditionally estimated the earth pressure that acts on structures using either Rankine's (1857) or Coulomb's (1773) theories. In engineering practice, the displacements are often controlled or limited by choosing a suitable safety factor, and an appropriate construction sequence can prevent excessive yielding [24].

There are numerous developments of specific numerical codes and their encouraging results. This research considers a circular shaft because circular diaphragm walls can endure significant hoop stresses and vertical bending moments when facing water and ground pressures because of spatial circumferential arching effects. Compared with a rectangular diaphragm wall, a circular diaphragm wall can exhibit better structure stability for its integral rigidity and less radial deformation or deflection [22].

Emmanuel Rukundo, *Graduate student;*
e-mail:emmanuelrukundo@my.swjtu.edu.cn
Shen Yusheng, *Professor*, ***Corresponding author;***
e-mail: sys1997@163.com
Zhou Pengfa, *Graduate student*, *e-mail: zpf@my.swjtu.edu.cn*
Zhu Shuangyan, *Graduate student*, *e-mail:906859248@qq.com*

Key Laboratory of Transportation Tunnel Engineering, Ministry of Education, Southwest Jiaotong University, Jinniu District, Chengdu, Sichuan P.R. China. 610036.

Currently, there are three kinds of methods to predict the deformation of the tunnel surrounding rock. That is the mathematical model method or empirical formula method [5], artificial intelligence and numerical simulation algorithm [8],[20].

The performance of the active earth pressure distribution caused by installing a circular vertical shaft has been investigated by several researchers using experimental or numerical analysis methods. Walz [21] studied the active earth pressure on a circular vertical shaft using a model shaft equipped with a cutting edge ring. Lade et al. [16] performed physical modelling in which a flexible rubber bag filled with liquid or gas replaces the excavated soil. The liquid or gas pressure was reduced in stages to simulate the excavation of the shaft.

Giovanni Spagnoli et al.[12] formulated the New equations for estimating radial loads on Deep shaft linings in weak rocks, Used an analytical method called the convergence-confinement method to calculate both the radial displacement associated with the construction of the shafts and the equivalent loads that the planned shaft support must guarantee.

A.McCracken et al. [1] carried out the Geotechnical risk assessment for large-diameter raise-bored shafts and found an increase in diameter of raise-bored shafts; however, comes the more significant potential for instability of the walls and advancing face of the raise.

G.Walton et al.[10] carried out an Investigation of shaft

stability and anisotropic deformation in a deep shaft in Idaho, United States. During construction, the geological conditions of the shaft led to stability issues which ultimately necessitated design modifications.

Alex Hall et al. [2] studied Mechanisms of deterioration in a bored raise in brittle rock. Found that four factors influence the rise's deterioration: stress change after excavation, local geological structure, slashing-induced stress changes, and scouring of the raise as it was cut and dumped down the raise as the broken rock. The findings help improve understanding of brittle rock failure, better understand the deterioration mechanisms for mechanical cut raises in hard rock, calibrating numerical models, and making better engineering decisions for ground support and precondition blasting to improve the health and safety of workers.

Liyun Yang et al. [17] carried out a Model experimental study on the effects of in situ stresses on pre-splitting blasting damage and strain development. In drilling and blasting in deep underground engineering, in situ stress is usually considered an essential factor for blasting parameter design. When the direction of the uniaxial pressure is perpendicular to the blast-hole layout's direction, the specimen's damage after blasting is substantial and is not conducive to the formation of cracks.

Ayberk Kaya et al. [3] carried out a Stability investigation of a deep shaft using different methods, investigated two service shafts using empirical analysis, analytical analysis and numerical simulation methods, concluded that these analysis methods, 2D FEM simulation is most compatible with the actual field data.

Additionally, using a mechanical system to move the vertical shaft to simulate soil displacement may occur during the excavation process. Several researchers [11],[14] have adopted simplified models to simulate the lining's radial displacement. Herten and Pulsfort [13] and Chun and Shin [6] modified previous models by considering radial symmetry to model only a portion of the structure

The empirical equations are heavily subjected to some significant limitations, including their applicability to different tunnel geometries, soil properties, and construction procedures [22]. The numerical analysis methods can take into account the coupling effects of some factors, such as the ground condition, shape of the excavation cross-section, and support conditions [15],[9],[19],[7]. So, a combination of different approaches can improve the design in the complex stress state.

The objective of this paper is to study the similarity of theoretical calculations and numerical analyses of the deep shaft for mountain tunnel based on the excavation approach and comprehensive parametric studies by varying the combinations of several key design factors to determine the appropriate factor of safety, secondary lining thickness and construction method.

1.1 Huayingshan tunnel shaft engineering

The shaft of the Huayingshan tunnel for the Nanchong-Dazhu-Liangping expressway is in Southwest China, the shaft depth is 335.732m, and the internal diameter is 8m.

According to the shaft (geology) vertical profile, the shaft bore passes through the interlacing surrounding rock of the grade III, IV and V with each other, as elaborated in Figure 1.

Grade III surrounding rock; its lithology is mainly medium-thick layered limestone with hard rock, and mudstone with thin layered limestone with soft rock, no development of joints, the rock mass is intact, no development of groundwater, the karst is not well developed, and there are no karst holes and fissures. The surrounding rocks are relatively complete as a whole.

Grade IV surrounding rock: its lithology is mainly thin to medium thick layered argillaceous limestone and thin layered soft marl, no groundwater in the rock joints and no karst in general. Only a few karst holes and with fissures locally. Surrounding rocks are generally fragmented and, in some sections, are easy to fall when cut against unfavourable joints.

Grade V surrounding rock: Its lithology is mainly composed of thin layered marl, muddy limestone and even very soft grey yellow mudstone. The joints are very developed, and the core is fragmental and pancake-like. No groundwater and the karst is not very developed, only a small amount of dissolved pore and with soluble parts.

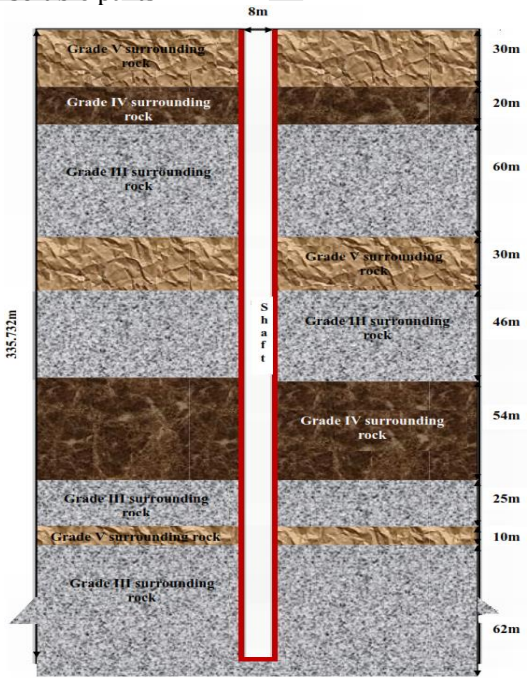

Fig.1: Huayngshan tunnel shaft geological profile

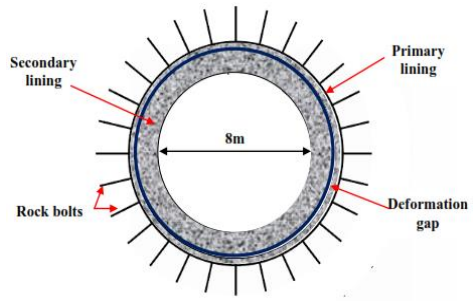

Fig. 2: Shaft cross-section

From Fig 2, the lining adopts a composite lining structure, according to the surrounding rock grade, shaft depth, formation lithology, and other factors like engineering analogy, finite element value analysis and the lining support parameters[23].

2. MATERIALS AND METHODS

Table 1: Physical parameters of support and surrounding rock

Properties	Surrounding rock grade			Primary support (C25)	Secondary lining (C35)
	III	IV	V		
Density (kN/m)	25.9	25.0	18.0	23.0	25.0
Modulus of elasticity (Gpa)	15.0	6.0	1.6	27.0	32.5
Poisson's ratio	0.20	0.28	0.36	0.22	0.20
Internal friction angle	45	36	23		
Cohesion (Mpa)	1.2	0.5	0.2		

The physical parameters of shaft lining support and surrounding rock grades are based on field tests, laboratory tests, and some Chinese code data to design road tunnels (2004).

2.1 Numerical analysis

Shaft calculation model establishment

The selection range of calculation is five times the shaft diameter(40m) in the X and Y direction; in the Z direction, the model height is 400m, and the excavation depth of the shaft is 335.732m. The boundary condition is the displacement boundary condition. The upper boundary to the ground is a free surface, the two sides parallel to the YOZ face are X-direction displacement constraints, the two sides parallel to the XOZ face are Y-direction displacement constraints, and the ground parallel to the XOY face is X, Y, Z-direction displacement constraints. The initial load is the self-weight load of the rock mass. Figure 3 is for cross-section and longitudinal profile.

The surrounding rock, primary support, and secondary lining are simulated by the adapted element, as shown in Figure 4. Adapt a full face mechanised excavation. The cyclic footage of grade V surrounding rock is 1m, that of grade IV surrounding rock is 2m, and that of grade III surrounding rock is 4m. After excavation, drive anchor bolts into the surrounding rock and complete the initial support in time.

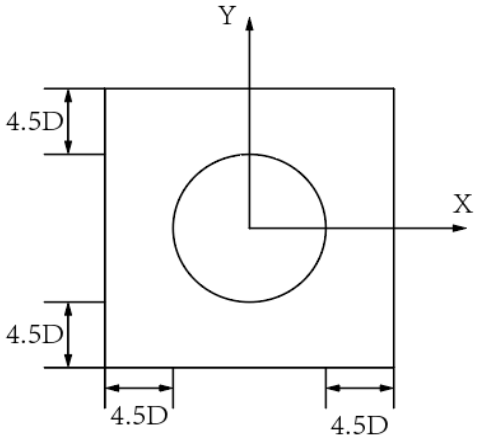

Fig.3(a) Cross-section

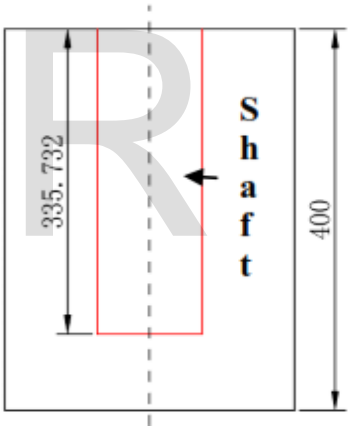

Fig.3(b) Longitudinal profile

Fig.3: Cross-section and longitudinal profile (units: m).

Note: SL – Secondary Linning.

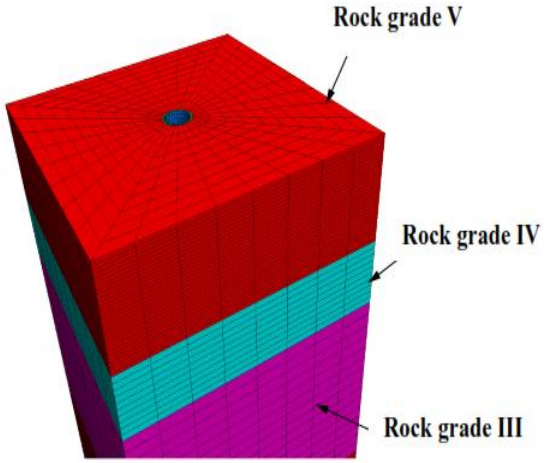

Fig.4(a) Surrounding rock grades

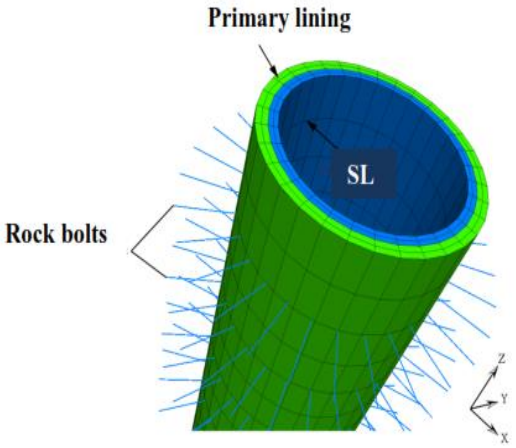

Fig.4b) Primary and secondary linings.
Fig. 4: The shaft simulation model

2.2 Concrete lining thickness (t_c) calculation

Concrete is among the existing lining support for circular excavations, as shown in Fig 5. A concrete cylinder subjected to a uniform pressure (radial) around its outer circumference develops internal compressive stress tangential to its circumference. If the pressure is applied suddenly, the concrete reacts elastically, and the stress near the interior wall of the lining is most significant and gradually reduce towards the outer wall (Vergne, 2003). For this case, Lame's thick wall formula gives the maximum support pressure of concrete [4]:

$$p_{sc\,max} = \frac{f_c}{2}\left[1 - \frac{r^2}{(r+t_c)^2}\right] \quad (1)$$

Where f_c is the uniaxial compressive strength of concrete, r is the inner radius, and t_c denotes lining thickness.

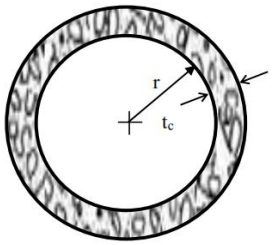

Fig. 5: Concrete lining for a circular shaft excavation.

From (1), estimate the thickness of concrete as

$$t_c = r\left(\sqrt{\frac{f_c}{f_c - 2p_{sc\,max}}} - 1\right) \quad (2)$$

If the pressure is tremendous and applied slowly, the concrete may react plastically, and the stresses tend to redistribute themselves evenly across the thickness of the concrete wall. Among several formulae developed to account for this plastic or visco-elastic property of concrete, the best one is Huber's formula (Vergne, 2003):

$$p_{sc\,max} = \frac{f_c}{\sqrt{3}}\left[1 - \frac{r^2}{(r+t_c)^2}\right] \quad (3)$$

Then, the thickness of concrete is

$$t_c = r\left(\sqrt{\frac{f_c}{f_c - \sqrt{3}p_{sc\,max}}} - 1\right) \quad (4)$$

The stiffness of concrete is

$$k_c = \frac{E_c\left[(r+t_c)^2 - r^2\right]}{(1+v_c)\left[(1-2v_c)(r+t_c)^2 + r^2\right]} \quad (5)$$

Where E_c is Young's modulus of concrete; v_c is Poisson's ratio for concrete.

For the analysis of circular shafts, prefer cylindrical coordinates, as shown in Figure 6, consider the opening long enough, and variations with **z** are negligible so that derivatives concerning **z** are zero. In particular, the z-direction strains are zero, and the analysis is a plane strain [18].

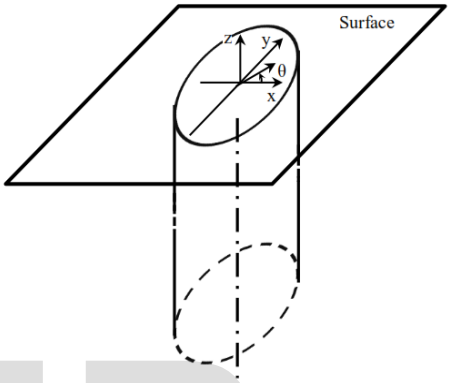

Figure 6: A circular shaft with coordinates (Pariseau, 1992).

The stresses around the shaft in Figure 6 after excavation are given by

$$\sigma_{rr} = \sigma_h\left(1 - \frac{r^2}{R^2}\right) \quad (6)$$

$$\sigma_{\theta\theta} = \sigma_h\left(1 + \frac{r^2}{R^2}\right) \quad (7)$$

$$\sigma_z = \gamma z \quad (8)$$

$$\sigma_h = k\sigma_z \quad (9)$$

Where σ_{rr} and $\sigma_{\theta\theta}$ are post-excavation stresses in the radial and circumferential (tangential) directions, respectively. σ_h and σ_z are pre-excavation horizontal and vertical stresses related by the constant k (horizontal to vertical stress ratio); z is depth; γ is the specific weight of rock; r is the shaft radius, and R is a questioned distance from the centre of the opening.

2.3 Safety factor determination

Amodel for a circular shaft lining loaded with water pressure and with a hollow (thick-walled) cylinder loaded by radial pressures p_a and p_b acting on the inside of the lining at a radius a and at the outside of the liner at a radius b (unlined shaft diameter $D_o = 2b$).

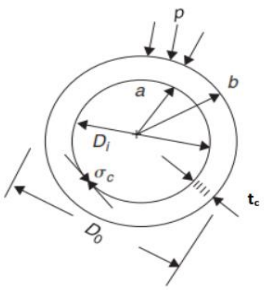

Fig. 7: A circular shaft lining model

From Fig. 7, the cylinder is considered elastic with Young's modulus E and Poisson's ratio $\boldsymbol{v}$ and under plane strain conditions (ϵ_{zz} = 0). The problem is also one of axial symmetry. Stresses, strains, and displacements are therefore independent of **z** and θ. Under these conditions, consider only the radial displacement u.

Where, if compression is positive, then a positive radial displacement is inward. In the usual case, there is no internal pressure p_a acting on the lining, so

$$\sigma_{rr} = \left(\frac{p_b}{1-\left(\frac{a}{b}\right)^2}\right)\left(1-\frac{a^2}{r^2}\right) \quad (10)$$

$$\sigma_{\theta\theta} = \left(\frac{p_b}{1-\left(\frac{a}{b}\right)^2}\right)\left(1+\frac{a^2}{r^2}\right) \quad (11)$$

$$u = \left(\frac{1+v}{E}\right)\left[(1-2v)\left(\frac{p_b}{1-\left(\frac{a}{b}\right)^2}\right)r + \left(\frac{p_b}{1-\left(\frac{a}{b}\right)^2}\right)\left(\frac{a^2}{r}\right)\right] \quad (12)$$

That is first satisfied where $\boldsymbol{r}$ is the least, that is, at $r = a$. At significant r, the left side of the failure criterion is too small to satisfy the equality.

Thus, lining failure initiates at the inside of the lining when

$$p_b = \left[\frac{(c)\cos(\emptyset)}{1-\sin(\emptyset)}\right]\left[1-\left(\frac{a}{b}\right)^2\right] \quad (13)$$

The circumferential stress on the inside of the lining ($r = a$) is maximum. Thus,

$$\sigma_{\theta\theta}(a) = \frac{2p_b}{1-\left(\frac{a}{b}\right)^2} \quad (14)$$

The radial stress is zero, as b becomes indefinitely large, the stress approaches two times the applied stress, which agrees with a circular hole under hydrostatic stress. If p_b is reference stress and K is a lining stress concentration factor, then;

$$\sigma_{\theta\theta} = Kp_b \quad (15)$$

$$K = \left[\frac{2}{1-\left(\frac{a}{b}\right)^2}\right] \quad (16)$$

The safety factor for the lining is given by

$$FS_c = \frac{C_o}{\sigma_c} = \frac{C_o}{Kp_b} = C_o\left[\frac{1-\left(\frac{a}{b}\right)^2}{2p_b}\right] \quad (17)$$

If the lining thickness t_c is specified, so that $t_c = b - a$, then the factor of safety may be calculated, given the lining strength C_o and applied stress p_b

Alternatively, calculate a lining thickness from a given safety factor or, equivalently, for a given maximum allowable stress ($C_o/F.S.$).

Two formulae are possible, one in terms of the inner lining radius a, the other in terms of the outer lining radius b, which is also the radius of the unlined shaft wall. Thus, after solving the lining safety factor equation,

$$t_c = b\left[1-\left(\frac{C_o-2p_b F.S.}{C_o}\right)^{\left(\frac{1}{2}\right)}\right] \quad (18)$$

$$t_c = a\left[\left(\frac{C_o}{C_o-2p_b F.S.}\right)^{\left(\frac{1}{2}\right)}-1\right] \quad (19)$$

Both follow directly from the lining safety factor formulae. In consideration of the square root operation, the lining load can, in no case exceed one-half of the unconfined compressive strength of the lining material. Lining loads from water pressure are an order of magnitude less, although there are notable exceptions.

In exceptional cases, a concrete lining alone may not suffice; combinations of steel and concrete are essential to support very high water pressure.

2.4 Construction mechanics

Consider a one meter run of shaft lining with internal radius a and external radius b in contact with the rock, as shown in Fig.8.

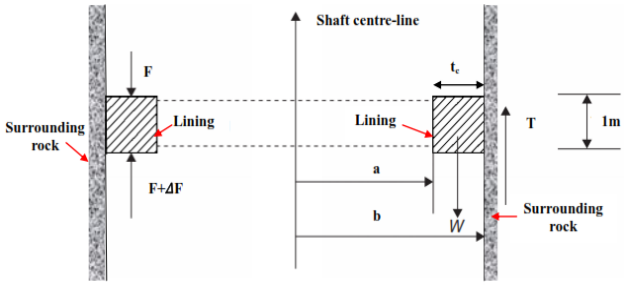

Fig. 8: Shaft lining model calculation

Fig.8 shows a ring in equilibrium with a shearing force acting on the perimeter of the ring at the concrete-rock contact with no change in vertical force from top to ring bottom; the shear force required for equilibrium is

$$W = T \quad (20)$$

$$\gamma\pi(b^2-a^2) = 2\pi b\tau \quad (21)$$

Where τ is the average shear stress acting over a one-meter run of the lining. Solution for τ gives

$$\tau = \frac{\gamma}{2b}(b-a)(b+a)$$

$$\tau \approx \frac{\gamma}{2b}(h)(2b)$$

$$\tau = \gamma t_c \quad (22)$$

Thus, shear stress required to support the lining is almost equal to the product of lining specific weight γ and lining thickness t_c. The weight of a concrete shaft lining poured to the shaft walls is not crucial to lining stress. Thus a slight bond strength between concrete and rock is sufficient to support the lining weight.

3. RESULTS AND DISCUSSIONS

3.1 Principal stress analysis of secondary lining

The surrounding rock 110m-140m away from the shaft-head is grade V, with poor surrounding rock conditions and considerable excavation depth. Therefore, selecting the shaft lining structure within 110m-140m away from the shaft-head as the representative section for analysis.

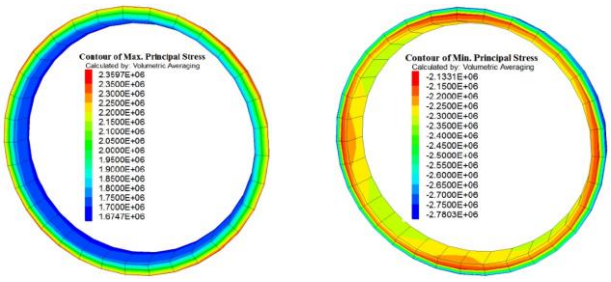

Fig.9(a): Maximum Fig.9(b): Minimum.

Fig. 9: Principal Stress diagrams of shaft lining structure 120m away from the shaft-head (Units: Pa)

It can be seen from Fig. 9 that at 120m from the shaft-head, the maximum value of the maximum principal stress of the lining is 2.36MPa, the maximum value of the minimum principal stress is 2.78MPa, the minimum value of the maximum principal stress of the lining is 1.67MPa, and the minimum value of the minimum principal stress is 2.13MPa. The maximum and minimum principal stresses are at the periphery of the lining, that is, the contact position with the primary support, and the minimum is at the inner side of the lining.

From (7), the maximum principal and minimum principal stresses (post-excavation stresses) are 2.79MPa and 1.58MPa, which approximately correlates with the simulation analysis's values. With maximum principal stress and (1), determine the concrete lining thickness t_c for the tunnel shaft.

3.2 Analysis of horizontal displacement of the surrounding rock

There are layers of grade III, IV and V surrounding shaft rocks. The unfavourable locations, i.e. 20m, 120m (V surrounding rock) and 210m (IV surrounding rock) from the shaft-head, are selected as representative sections for analysis. Below are displacement cloud charts.

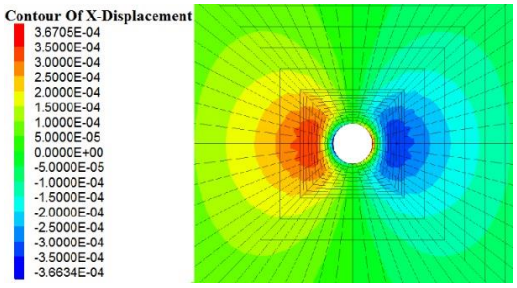

Fig.10(a) At 20m

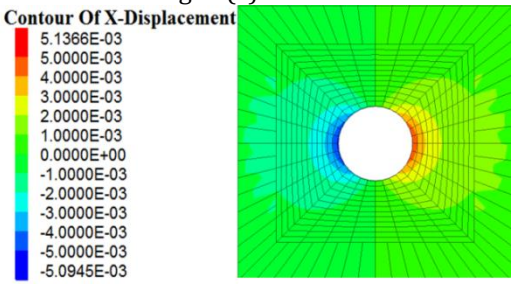

Fig.10(b) At 120m

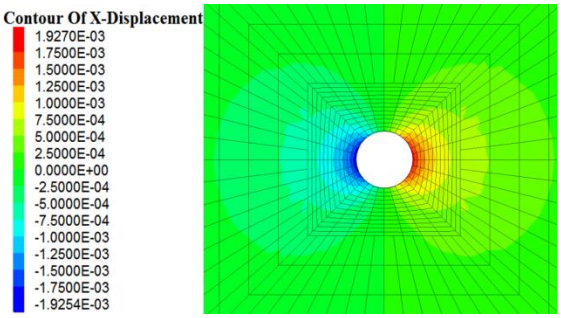

Fig.10(c) At 210m

Fig. 10: Horizontal displacement diagrams of surrounding rock at different locations (units: m).

From Fig. 10, the horizontal displacement change rule is the same. The displacement decreases continuously with the increase of the distance between the surrounding rock and the shaft wall. The surrounding rock's substantial horizontal displacement is 5mm at 120m, followed by 2mm at 210m and a minimum at 20m from the shaft-head (see fig.11).

From (12) and (13), determine the change in inside diameter (radial displacement)when the load is sufficient to cause lining failure.

From either (1) or (14), the maximum support pressure or contact pressure at the verge of failure for rock grade v (120m) is 2.73MPa and rock grade IV (210m) is 2.5MPa with the displacement of 6.1mm from (12).

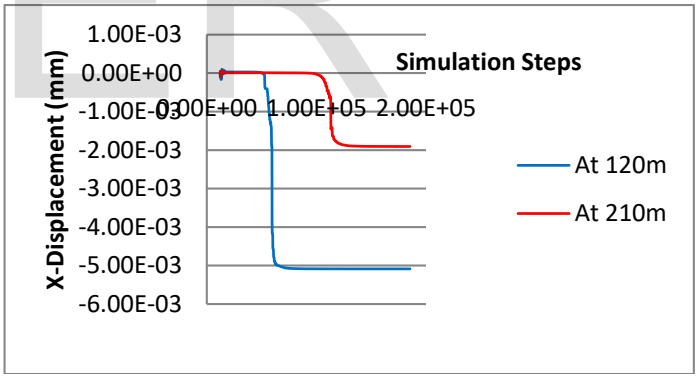

Fig 11: Horizontal displacement curve of the surrounding rock at 120m and 210m

3.4 Vertical stress distribution of soft-hard rock interfaces

Due to the surrounding rock's complex geological conditions, the shaft is, with the interlacing of the grade III, IV, and V surrounding rock. In some sections, the grade III surrounding rock transits directly to the grade V surrounding rock, as shown in Fig.12. When passing through the soft-hard rock interface, it is necessary to analyse the mechanical characteristics during the shaft excavation.

This section compares the construction of the grade III surrounding rock and the grade V surrounding rock at the soft-hard interface; Comparing and analysing the secondary lining.

a). Lining structure stress of grade III surrounding rock (109m) towards the interface.

b). Lining structure stress at the interface (110m); At 1-1

interface, grade III surrounding rock transits to grade V surrounding rock.

c). Stress diagram of lining structure of grade V surrounding rock (112m) after the interface

d). Stress diagram of lining structure of grade V surrounding rock (138m) towards the interface.

e). Lining structure stress at the interface (140m); At 2-2 interface, grade V surrounding rock transits to grade III-surrounding rock.

f). Grade III surrounding rock after the interface (141m) lining structure stress.

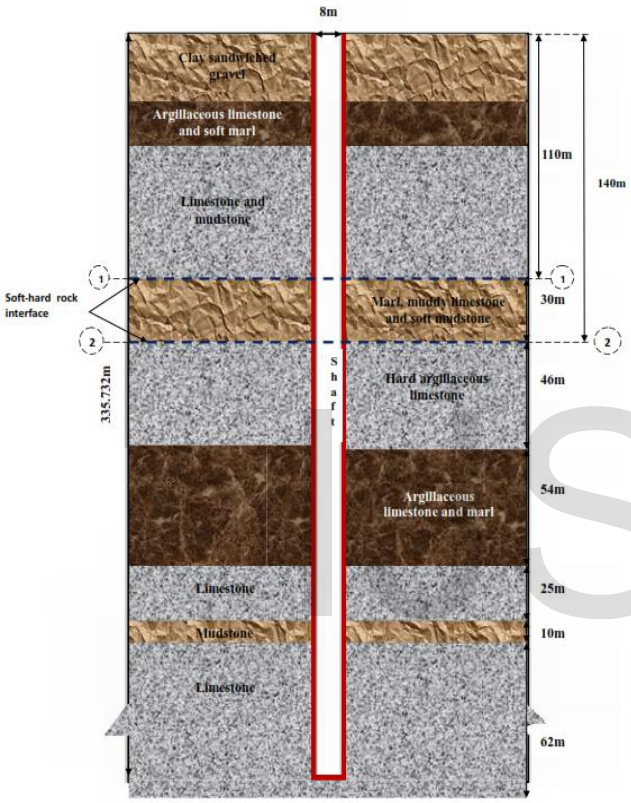

Fig.12: Lining principal stress analysis at soft-hard surrounding rock interfaces

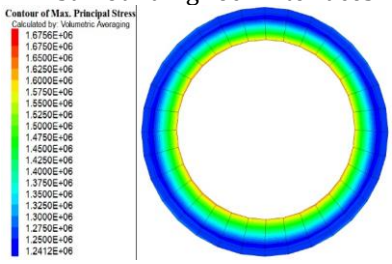

Fig.13(a): At 109m

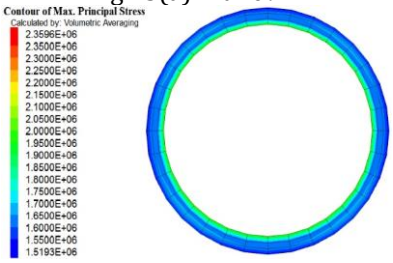

Fig.13(b): At 110m.

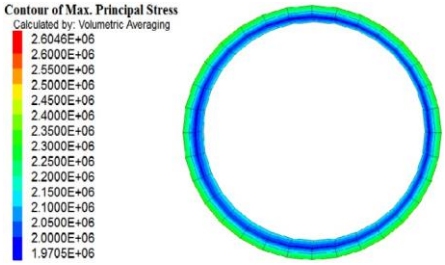

Fig.13(c): At 112m.

Cross-section 1-1 Max. Principal stress

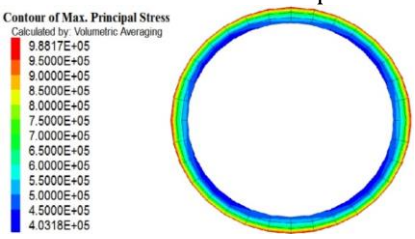

Fig.13(d) At 138m

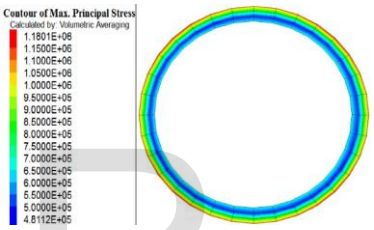

Fig.13(e) At 140m

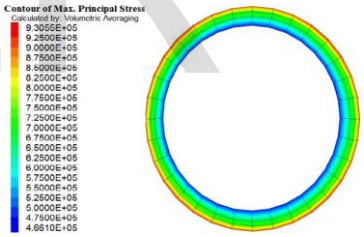

Fig.13f): At 141m.

Cross-section 2-2 Max. Principal stress

Fig. 13: Principal stress analysis of soft-hard lining interfaces below shaft-head(Units: Pa)

Table 2: Summary of maximum principal stress results at selected points.

Rock Grade / Interface	III	Interface	V	V	Interface	III
Depth (m)	109	110	112	138	140	141
Max. Principal Stress (MPa)	1.68	2.36	2.60	0.99	1.18	0.93

From Fig. 13 and Table 2, the maximum stress is 2.36MPa at the soft-hard interface of grade III surrounding rock at 110m away from the shaft-head, while at the grade III surrounding

rock at 1m above the soft-hard interface, the maximum stress is 1.68MPa, and at the grade V surrounding rock at 2m below the soft-hard interface, the maximum stress is 2.60MPa.

At the interface 140m away from the shaft-head (soft-hard surrounding rock interface), the maximum stress is only1.18MPa, while the maximum stress of grade III surrounding rock 1m below the soft-hard interface is only 0.93MPa, and the maximum stress of grade V surrounding rock 2m above the soft-hard interface is only 0.99MPa. Refer to Fig.14 for more elaboration.

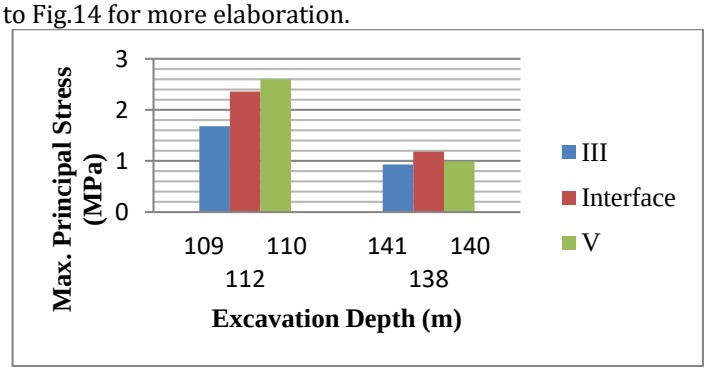

Fig.14: Maximum principal stress results at selected monitoring points.

The lining stress values at the interface and grade V surrounding rock are slightly higher than that at the transition section of grade III surrounding rock. The stress values' difference is not significant; with the maximum stress of 2.6MPa from the numerical analysis, the lining structure is safe since the maximum stress is 10.83MPa from (17) at the verge of lining failure.

Considering monitoring points maximum principal stress values, with the value of compressive stress of concrete, and from (14), the pressure at lining failure can be determined and then values inserted in (1) to determine the lining thickness t_c of the tunnel shaft.

3.5 Plastic zone distribution of the surrounding rock

The plastic area of surrounding rock during shaft excavation at the cross-section 20m, 120m and 210m away from the shaft-head are representative cross-sections.

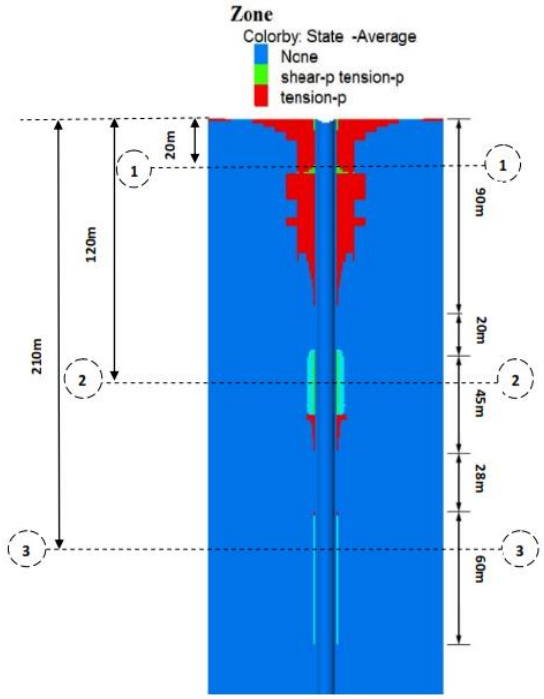

Fig. 15: Vertical profile plastic zone of the surrounding rock.

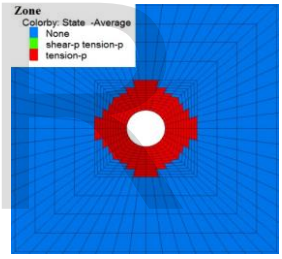

Fig.16(a) Cross-section 1-1 At 20m.

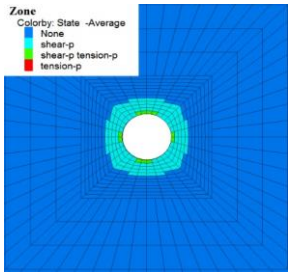

Fig.16(b) Cross-section 2-2 At 120m.

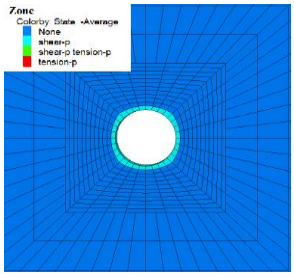

Fig.16(c): Cross-section 3-3 At 210m.

Fig. 16: Plastic zones of representative sections below the shaft-head.

From Fig.15 and Fig.16, during shaft excavation, the plastic area is more near the shaft-head, and the far away from the shaft-head, the smaller the plastic area; the plastic area is more extensive at grade V surrounding rock, followed by grade IV surrounding rock, and the condition of grade III surrounding rock is better no plastic area.

The contact pressure values between lining and rock on the verge of failure for rock grade V (at 20m and 120m), rock grade IV (at 210m) and rock grade III are 2.73MPa, 2.50MPa and 2.01MPa, respectively from equation 14. The maximum pressure values to cause severe plasticity of the lining from rock grade III (at 20m and 120m), rock grade IV (at 210m) and rock grade III are 3.15MPa, 2.88MPa and 2.32MPa, respectively from (3).
Therefore the shaft lining structure is okay since the contact pressure values that can cause the shaft lining structure to fail are less than the maximum pressure values to cause severe plasticity of the lining structure.

3.6 The safety factor of the shaft wall
Use the load-structure method to calculate the stress on the shaft wall. The lining material is C35 concrete and simulated by beam element, with surrounding strata, equivalent to spring structure, simulated by link10 element. Take the spring length as 1m in the calculation, as shown in Fig.17.
NB: The numbers in fig. indicate the node number in ANSYS calculation.

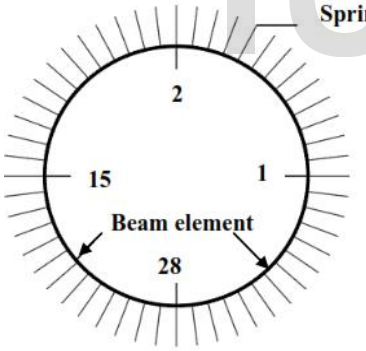

Fig. 17: Calculation model of the ANSYS load structure

3.6.1 Vertical profile analysis results at 140m below shaft head
The excavation depth at 140m below shaft-head, and the surrounding rock grade is grade V. the reaction coefficient of the surrounding rock is 250MPa/m, and the side pressure of surrounding rock is 1.06MPa. Through the modelling and calculation by ANSYS, Fig.18(a), Fig.18(b) and Fig.18(c) respectively show the axial force, bending moment and safety factor of shaft lining structure under the action of surrounding rock pressure when the excavation depth is 140m.

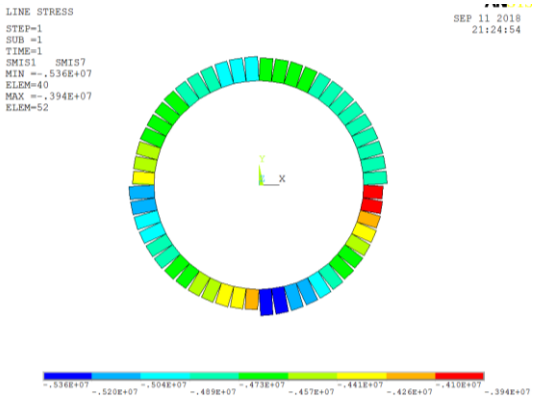

Fig.18(a) Axial force diagram (Units: N)

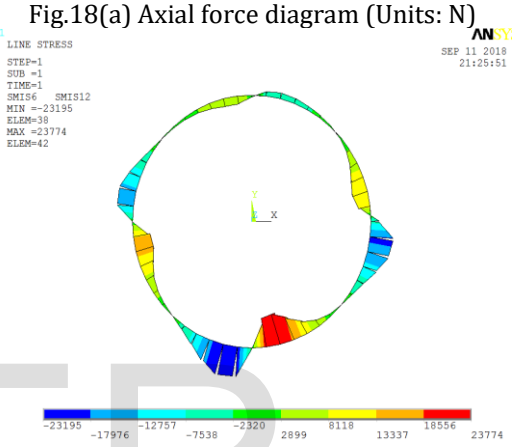

Fig.18(b) Bending moment diagram(Units: Nm)

Fig.18: Axial force and Bending moment diagrams at 140m below shaft-head.

The surrounding rock load distribution is evenly around the shaft lining structure from analysis and observation of Fig. 18(a) and Fig.18(b). The axial force distribution on the linning structure is also relatively uniform. The maximum axial force is 5360Kn, which appears at node 28 of the lining structure.

Due to the structural alignment, the bending moment and axial force are also symmetrical. The maximum value of the bending moment is 0.024MNm, and the approximate position is consistent with the maximum position of axial force.
NB: S.F – Safety factor.

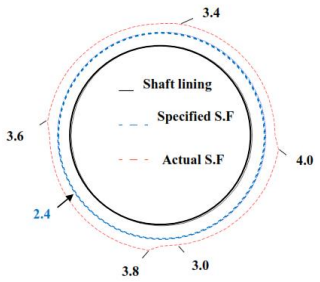

Fig. 18(c): Safety factor of lining structure at 140m below shaft-head.

From Figure 18c, the factors of safety of shaft lining structure are higher than the specified value of safety factor by 2.4. The maximum value of the safety factor appears near node one; the

maximum value is 4.0, the minimum value of safety factor appears at node 28, and the minimum value is 3.0, indicating that the shaft lining structure buried at 140m is safe and stable. Since from Equation 17, the safety factor is 2.6, and the shaft lining thickness tc is 0.46m from Equation 19.

3.6.2 Vertical profile calculation results at 260m below shaft-head

Through the modelling and calculation by ANSYS, Figure 19(a) and Fig.19(b) respectively show the axial force and bending moment diagrams of shaft lining structure under the action of surrounding rock pressure when the excavation depth is 260m.

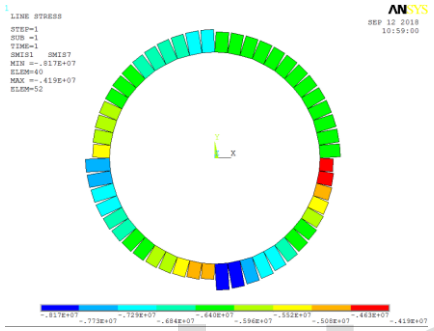

Fig.19(a): Axial force diagram(Units: N)

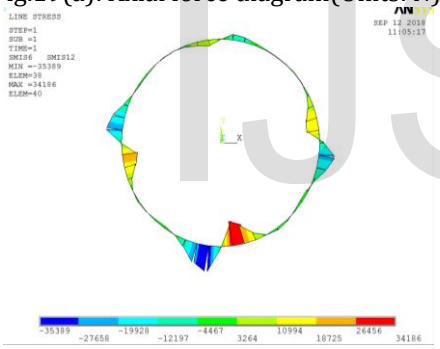

Fig.19(b) Bending moment diagram (Units: Nm)

Fig.19: Axial force and Bending moment diagrams at 260m below the shaft-head

Fig.19(a) and Fig.19(b) show that the surrounding rock load distribution is evenly around the shaft lining structure. So the axial force distribution on the linning structure is also relatively uniform; the maximum axial force is 8170kN, which appears at the left and right of node 28 of the lining structure;

Because of the structure's symmetry, the bending moment and axial force also present an asymmetrical form, and the maximum bending moment is 0.034MNm, approximate position and axis; the maximum position of the force matches.

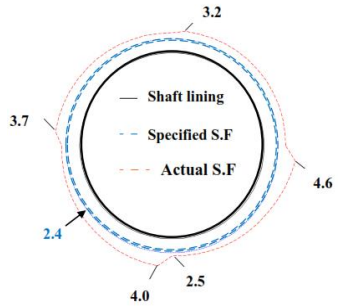

Fig. 19(c): Safety factor of lining structure 260m below shaft-head.

From Fig.19 (c) that the safety factors of shaft lining structure are higher than the specified safety factor value of 2.4, the maximum value of safety factor appears near node 1, the maximum value is 4.6, the minimum value of safety factor appears at node 28, and the minimum value is 2.5, indicating that the shaft lining structure buried at 260m is safe and stable.

The safety factors of lining structure at 140m and 260m below the shaft-head are higher than the specified value of safety factor by 2.4, indicating that the lining support parameters meet the requirements of construction safety. Because the surrounding rock conditions at 20m are similar to that at 140m. However, because the excavation depth of 20m is shallow and the surrounding rock's lateral pressure is small, when the section at 140m below shaft-head meets the safety requirements, the section at 20m also meets the requirements.

3.7 Stress analysis of lining structure vertically

The excavation depth of the shaft is 335.732m, and extract the maximum stress during the construction of some points on the lining structure to obtain the stress curve.

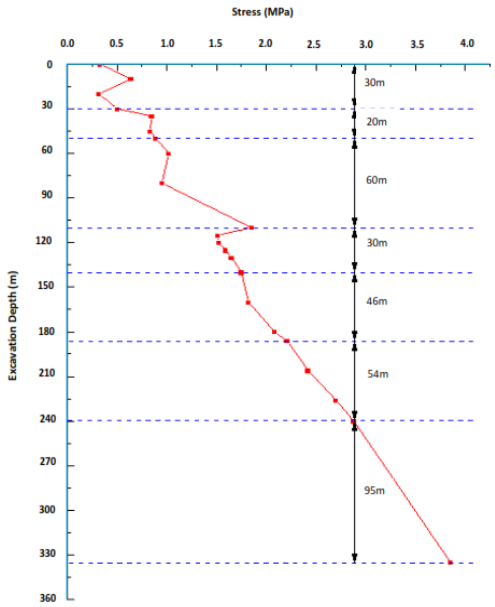

Fig. 20: Vertical profile stress curve of lining structure.

Table 3: Stress at monitoring points of lining structure.

Excavation Depth (m)	10	30	50	110	140	186	240	335
Stress (MPa)	0.64	0.5	0.89	1.85	1.75	2.21	2.88	3.85

Table 3 and Fig. 20 show that the maximum stress in the construction process increases with the increase of the excavated depth, and the lining structure's stress increases continuously. The maximum value is 3.85MPa at the most profound excavated depth, and there are various degrees of stress mutations at the depth 30m, 50m, 110m and 140m away from the shaft -head, more notably at the position with the excavated depth of 110m, which is just the location where the grade III surrounding rock transits to the grade V surrounding rock. The rock stiffness does not match, and the stress suddenly changes.

4. CONCLUSIONS

The lining structure's safety factors calculated from numerical analyses and theoretical calculations at all selected points below the shaft-head are higher than the specified value of safety factor of 2.4, indicating that the lining support parameters meet construction safety requirements.

The numerical analysis method can consider the coupling effects of factors, such as varying rock properties and different construction procedures. The secondary lining thickness kept on varying because of interlacing surrounding rock grades exerting a varying pressure on the secondary lining; therefore, using In-situ concrete or cast in place linings for lining construction is more suitable.

The weight of a concrete shaft lining poured to the shaft walls is not crucial to shaft bottom-lining stress because a slight bond strength between concrete and rock is sufficient to support the lining weight. Hence underpinning technique of shaft construction is more appropriate.

ACKNOWLEDGEMENT

This study was supported by the National Natural Science Foundation of China (No. 51778540, No. 51678501).

REFERENCES

[1] A. McCracken et al. Geotechnical risk assessment for large-diameter raise-bored shafts, Shaft Engineering conference, organised by the Institution of Mining and Metallurgy in association with the Institution of Civil Engineers, the Institution of Mining Engineers, and held in Harrogate, England, from 5 to 7 June 1989 PP 322-331.

[2] AlexHall et al. Mechanisms of deterioration in a bored raise in brittle rock. International Journal of Rock Mechanics and Mining Sciences, March 2021, Volume 139.

[3] Ayberk Kaya et al., Stability investigation of a deep shaft using different methods, International Journal of Geomechanics, February 2021, Volume 21, Issue 2

[4] Brady, B. G., & Brown, E. T. (2005). Rock Mechanics for Underground Mining. New York: Kluwer Academic Publishers.

[5] Chou and Bobet, Predictions of ground deformations in shallow tunnels in clays, Tunnelling and Underground Space Technology, January 2002, Volume 17, Issue 1, Pages 3-9.

[6] Chun, B.S., Shin, Y.W., Active earth pressure acting on the cylindrical retaining wall of a shaft. South Korea Ground Environ. Eng., 2006, J. 7 (4), 15-24.

[7] Do, N.A., Dias, D., Oreste, P., Djeran-Maigre, I., 2014. Three-dimensional numerical simulation of a mechanised twin tunnel in soft ground. Tunnelling. Undergr. Space Technol.

[8] Fargnoli et al. Twin tunnel excavation in coarse-grained soils: Observations and numerical back-predictions under free field conditions and in presence of a surface structure, Tunnelling and Underground Space Technology, June 2015, Vol 49, Pages 454-469.

[9] Funatsu, T., Hoshino, T., Sawae, H., Shimizu, N., 2008. Numerical analysis to better understand the mechanism of the effects of ground supports and reinforcements on tunnels' stability using the distinct element method. Tunnelling Undergr. Space Technol. 23 (5), 561-573.

[10] G.Walton et al. Investigation of shaft stability and anisotropic deformation in a deep shaft in Idaho, United States, International Journal of Rock Mechanics and Mining Sciences, Volume 105, May 2018, Pages 160-171.

[11] Ghareh and Saidi, An investigation on the behaviour of retaining structure of excavation wall using obtained results from numerical modelling and monitoring approach. (A case study of international “Narges Razavi 2 Hotel”, Mashhad), Journal of Structural Engineering & Geotechnics, 2011, Vol 1, Issue 2, Pages 17-23.

[12] Giovanni Spagnoli et al., New equations for estimating radial loads on Deep shaft linings in weak rocks, International Journal of Geomechanics, December 2016, Volume 16, Issue 6

[13] Herten, M., Pulsfort, M., 1999. Determination of spatial earth pressure on circular shaft constructions. Granular Matter 2 (1), 1-7.

[14] Imamura, S., Nomoto, T., Fujii, T., Hagiwara, T., 1999. Earth pressures acting on a deep shaft and the movements of adjacent ground in the sand. In: Proceedings of the International Symposium on Geotechnical Aspects of Underground Construction in Soft Ground, Tokyo, Japan, pp. 647-652.

[15] Karakus, M., Fowell, R.J., 2003. Effects of different tunnel face advance excavation on the settlement by FEM. Tunnelling Underground Space Technology. Incorporated. Trenchless Technology Res. 18 (5), 513-523.

[16] Lade, P.V., Jessberger, H.L., Makowski, E., Jordan, P., 1981. Modelling of deep shafts in centrifuge test. In: Proceedings of the International Conference on Soil Mechanics and

Foundation Engineering, Stockholm, Sweden, volume 1, pages 683-691.

[17] Liyun Yang et al. Model experimental study on the effects of in situ stresses on pre-splitting blasting damage and strain development. International Journal of Rock Mechanics and Mining Sciences, Volume 138, February 2021.

[18] Pariseau, W. G., 1977. Estimation of support Load Requirements for Underground Mine Openings by Computer Simulation of the Mining Sequence. Transactions. SME/AIME, Vol. 262, pp. 100 - 109.

[19] Sousa, J.A.E., Negro, A., Fernandes, M.M., Cardoso, A.S., 2010. Three-dimensional non-linear analyses of a metro tunnel in São Paulo porous clay Brazil. J. Geotech. Geoenviron. Engng. 137 (4), 376-384.

[20] Talebinejad et al., Investigation of surface and subsurface displacements due to multiple tunnels excavation in the urban area, Arabian Journal of Geosciences, 2014, Volume 7, Pages 3913-3923.

[21] Walz, B., 1973. Left bracket apparatus for measuring the three-dimensional active soil pressure on around model caisson right bracket. Baumaschine Bautechnik 20 (9), 339-344.

[22] Wang, H.N., Chen, X.P., Jiang, M.J., Song, F., Wu, L., 2018. The analytical predictions on displacement and stress around shallow tunnels subjected to surcharge loadings.Tunnelling. Undergr. Space Technol. 71, 403-427.

[23] Wickham et al., Support determinations based on geological predictions, N Am Rapid Excav & Tunnelling Conf Proc, 1972, Vol 1, Pages 43-64

[24] Wong, R.C.K., Kaiser, P.K., 1988. Design and performance evaluation of vertical shaft: rational shaft design method and verification of the design method. Can. Geotech. J. 25, 320-337.